

Real-time dual-wavelength digital holographic microscopy with a single hologram

Jonas Kühn^a, Tristan Colomb^{a,b}, Frédéric Montfort^c, Florian Charrière^a, and Christian Depeursinge^a

^aEcole polytechnique fédérale de Lausanne, Institute of imaging and applied optics, CH-1015 Lausanne, Switzerland;

^bCentre de Neurosciences Psychiatriques, Département de psychiatrie DP-CHUV, Site de Cery, 1008 Prilly-Lausanne, Switzerland;

^cLyncée Tec SA, PSE-A, CH-1015 Lausanne

ABSTRACT

We report on a method to achieve real-time dual-wavelength digital holographic microscopy with a single hologram acquisition. By recording both interferograms from two laser sources at different wavelengths in only one spatially-multiplexed digital hologram, we are able to independently propagate and apply numerical corrections on both wavefronts in order to obtain a beat-wavelength phase map of the specimen. This beat-wavelength being up to 10-100 times larger than the original wavelengths, we are in a situation where the 2π phase ambiguity of conventional DHM is removed and the phase measurement range of the technique is extended up to several tens of microns in height. The unique capability to perform such an operation with a single acquisition enables real-time dual-wavelength DHM measurements. Results on a moving micro-mirror are presented in this paper. We think that such a real-time dual-wavelength method represents a strong improvement to the current DHM state-of-the-art, and that it opens a whole new field of applications for this technique.

Keywords: Digital holography, dual-wavelength, two-wavelengths, beat-wavelength, microscopy

1. INTRODUCTION

Digital holography has experienced massive developments in the past years [1–3] as charge coupled device (CCD) and digital image processing technologies progressed. Similarly to classical holography [4], it enables to retrieve the object complex wavefront, both in amplitude and especially in phase, but in a quantitative way thanks to the numerical reconstruction with a computer. Digital holographic microscopy (DHM) uses a microscope objective (MO) to magnify the specimen and provides reconstructed images with a diffraction-limited lateral resolution down to a few hundreds of nanometers depending on the MO numerical aperture (NA), while the axial resolution is less than $\lambda/150$ due to the interferometric precision of the method [5]. However, this phase information is by essence only defined modulo 2π , so that optical path lengths (OPL) larger than one time the wavelength cannot be unequivocally measured, resulting in a so-called phase ambiguity and presence of phase jumps (wrapped phase). Usually phase unwrapping algorithms can be applied on this wrapped phase images to retrieve the true OPL map of the sample, but high aspect-ratio objects, such as specimens with step height where no phase jumps are present, or high roughness surfaces, as well as noisy experimental conditions can make such algorithms failing. Let us also point out that such unwrapping methods are often time-consuming, limiting applications to real-time measurements.

A well-known solution to this single-wavelength phase ambiguity is to combine two wavelengths to create a so-called beat-wavelength with a frequency equal to the frequency difference between them. Typically with visible-range wavelengths one can obtain micro- or millimeter-range beat wavelengths depending on the wavelength difference. In digital holography, this principle was first introduced by Wagner *et al.* [6] by subtraction of two in-focus reconstructed phase maps obtained with a scanning dye laser to perform a millimeter contouring of

Further author information: (Send correspondence to Jonas Kühn)
E-mail: jonas.kuehn@a3.epf.ch, Telephone: +41 21 693 37 42

the object. In recent works, similar DHM techniques to remove the phase ambiguity of digitally-propagated wavefronts by phase maps subtraction were published [7, 8]. These approaches usually require achromatic optics, otherwise numerical image resizing is needed, like the methods of Refs. [9] and [10]. Other digital holography works on these issues include the use of a laser diode mode-hop to change the wavelength [11] or the generation of a millimeter-range wavelength with a terahertz source [12, 13].

Nevertheless, all the previous two-wavelengths digital holography methods require a sequential approach to record the interferograms from both sources, with separated acquisitions for each wavelength. Consequently real-time dual-wavelength measurements are not possible because at least two camera acquisitions are needed, which is a strong limitation for e.g. monitoring moving samples or measuring in presence of vibrations. In this paper, we demonstrate that multi-reference waves DHM is a solution to overcome these drawbacks. The principle of multiple reference arms was introduced in classical holography by Lohmann in 1965 in Ref. 14 where a spatial multiplexing of wavelengths (also presented in Refs. 15–17) and of polarization is proposed. This methodology was applied in digital holography for polarization imaging by spatial multiplexing with two different orthogonally polarized reference waves [18–20], and also for multiple illumination angles in endoscopic digital holography [21, 22]. Here, we show that a dual-wavelength spatial multiplexing in digital holography enables single-acquisition beat-wavelength measurements and provides an ideal solution to compensate for chromatic aberrations.

2. PRINCIPLE

The principle is based on the acquisition of a hologram by a digital camera, with two collinear object beams \mathbf{O}_1 and \mathbf{O}_2 at two different wavelengths λ_1 and λ_2 that interfere with their two reference beams counterparts \mathbf{R}_1 and \mathbf{R}_2 , emitted by the same pair of laser sources, in a off-axis configuration (slight angle between object and reference beams). The expression for the intensity pattern, which results from an incoherent addition of both interferograms at λ_1 and λ_2 , can be written as

$$I_H(x, y) = |\mathbf{R}_1|^2 + |\mathbf{O}_1|^2 + |\mathbf{R}_2|^2 + |\mathbf{O}_2|^2 + \mathbf{R}_1 \mathbf{O}_1^* + \mathbf{R}_1^* \mathbf{O}_1 + \mathbf{R}_2 \mathbf{O}_2^* + \mathbf{R}_2^* \mathbf{O}_2, \quad (1)$$

with I_H being the hologram intensity, x , y the coordinates in the camera plane and $*$ denoting the complex conjugate.

In Eq. 1 the first four intensity terms are the zero order, which can be directly filtered in the Fourier domain [23], and the last four are the interference terms with the object wavefronts \mathbf{O}_i (the virtual images), or their conjugate \mathbf{O}_i^* (the real images), being modulated by the interference fringes spatial frequency (the carrier frequency) in the spatial frequency domain. With the object beams \mathbf{O}_i collinear on the optical axis, these carrier frequencies are dependent on the k-vectors of \mathbf{R}_1 and \mathbf{R}_2 . Now if the two references waves have different propagation directions, especially in the configuration where their k-vector projections on the CCD plane are orthogonal, each interference term occupies different position in the Fourier domain. Providing that there is no overlap between interference terms, a condition which imposes restrictions regarding the spatial frequency content of the object spectrum, it is therefore straightforward to isolate each frequency component by spatial filtering [23]. Afterwards, the only remaining operation is to numerically propagate in a separate manner the two associated wavefronts, as successfully done for polarization imaging with digital holography [18–20] or multiple angles endoscopic digital holography [21, 22]. Here the two interference terms of interest are $\mathbf{R}_1^* \mathbf{O}_1$ and $\mathbf{R}_2^* \mathbf{O}_2$, which have to be spatially filtered independently.

Writing these two filtered holograms as $I_{H,1}^F$ for $\mathbf{R}_1^* \mathbf{O}_1$ and $I_{H,2}^F$ for $\mathbf{R}_2^* \mathbf{O}_2$ and by using the convolution formulation, we have the following expression for the propagation in the Fresnel approximation:

$$\Psi_{\text{CF},i}(m, n) = \Gamma_i^I(m, n) \cdot \frac{\exp(i2\pi d_i/\lambda_i)}{i\lambda_i d_i} \cdot \text{FFT}^{-1} \left\{ \text{FFT} [\Gamma_i^H(k, l) I_{H,i}^F(k, l)] \cdot \exp \left\{ -i\pi \lambda_i d_i \left[\left(\frac{k}{N\Delta x} \right)^2 + \left(\frac{l}{N\Delta y} \right)^2 \right] \right\} \right\}, \quad (2)$$

where $\Psi_{\text{CF},i}$ is the reconstructed wavefront for wavelength λ_i in the convolution formulation, Γ_i^I and Γ_i^H are digital phase masks (DPM) in the image plane and in the hologram plane respectively, used to compensate for aberrations (see Ref. [24] for details), d_i is the propagation distance for wavelength λ_i , FFT is the Fast Fourier Transform operator, (k, l) and (m, n) are the couple of integers so that $(-N/2 < k, l, m, n \leq N/2)$ representing coordinates in the hologram plane, respectively the reconstruction plane, $N \times N$ is the number of pixels of the CCD camera and Δx and Δy are the pixel sizes.

The formulation of Eq. 2 enables to propagate numerically each wavefront $\Psi_{\text{CF},i}$ in parallel and in an independent manner. Moreover, the DPMs can be adapted to compensate for each wavefront aberrations and the propagation distances d_i can be adjusted differently to compensate for slight chromatic aberrations or axial specimen displacement. In top of that, the DPMs could also serve as digital magnification lenses to match the image sizes in case of stronger chromatic aberrations [9]. The parallel propagations yield a reconstruction rate of about 7 frames per second with a standard dual-core PC at 2 GHz with 512x512 pixels holograms (roughly half the standard single-wavelength reconstruction rate). A a-posteriori hologram stack reconstruction can also be performed and in this case is only limited by the acquisition rate of the CCD camera (here 25 frames per second). As said above, the reconstructed complex wavefronts \mathbf{O}_1 and \mathbf{O}_2 in the reconstruction plane contain information both in amplitude and in phase, providing a nanometer-scale resolution in the vertical axis, but are suffering from phase ambiguity for OPLs larger than the wavelength. However, the calculation of $\mathbf{O}_1 \mathbf{O}_2^*$ in the reconstruction plane allows to compute a synthetic beat-wavelength phase according to the following expression:

$$\Phi = \arg(\mathbf{O}_1 \mathbf{O}_2^*) = \phi_1 - \phi_2 = 2\pi \frac{x}{\lambda_1} - 2\pi \frac{x}{\lambda_2} = 2\pi x \left(\frac{\lambda_2 - \lambda_1}{\lambda_1 \lambda_2} \right) = 2\pi \frac{x}{\Lambda}, \quad (3)$$

where x is the OPL (twice the topography in reflection, for an homogeneous sample in air), ϕ_i the reconstructed phase for the wavelength λ_i and Λ is the synthetic beat wavelength defined as:

$$\Lambda = \frac{\lambda_1 \lambda_2}{\lambda_2 - \lambda_1}. \quad (4)$$

The interesting fact is that this beat wavelength is much larger than the original couple of wavelengths, the smaller the difference $(\lambda_2 - \lambda_1)$, the larger the synthetic wavelength, typically within the range of micrometers to millimeters. The corresponding synthetic phase obtained with Eq. 3 now enables to resolve much higher structures by removing the phase ambiguity in the range of the beat wavelength Λ , thus greatly increasing the range for the phase measurement. Thanks to the simultaneous recording approach exposed here, if we compute the phase difference Φ (Eq. 3) for each reconstructed hologram, it becomes possible to measure, in real time, the object under investigation as if a source of wavelength Λ were used.

Let us remind, though, that a great attention should be paid to the two laser sources stability as it is a top-priority issue when working with the expressions of Eq. 3 and 4 [25]. Indeed, any variations in wavelength is amplified when the beat wavelength phase map is computed, and the phase noise for ϕ_1 or ϕ_2 is also amplified when converted in topography due to the important value of Λ . To minimize these effects, high stability laser sources are required as well as careful setup design to minimize noise sources and use of low temporal coherence sources to avoid parasitic interferences.

3. EXPERIMENTAL CONFIGURATION

The setup we use for real-time dual-wavelength DHM is depicted in Fig. 1. The laser sources are two temperature-stabilized semiconductor laser diodes at $\lambda_1 = 679.57\text{nm}$ and $\lambda_2 = 759.91\text{nm}$, yielding $\Lambda = 6.428\mu\text{m}$ for the synthetic beat wavelength according to Eq. 4. The diodes wavelength stability was checked with a wavemeter, resulting in a wavelength deviation smaller than 10pm over 8h . The corresponding measurement error for a $3\mu\text{m}$ high step (nearly $\Lambda/2$), caused by a change of Λ , is less than 1\AA . The diodes also emit a low coherence (coherence length about 0.3mm) linearly polarized light.

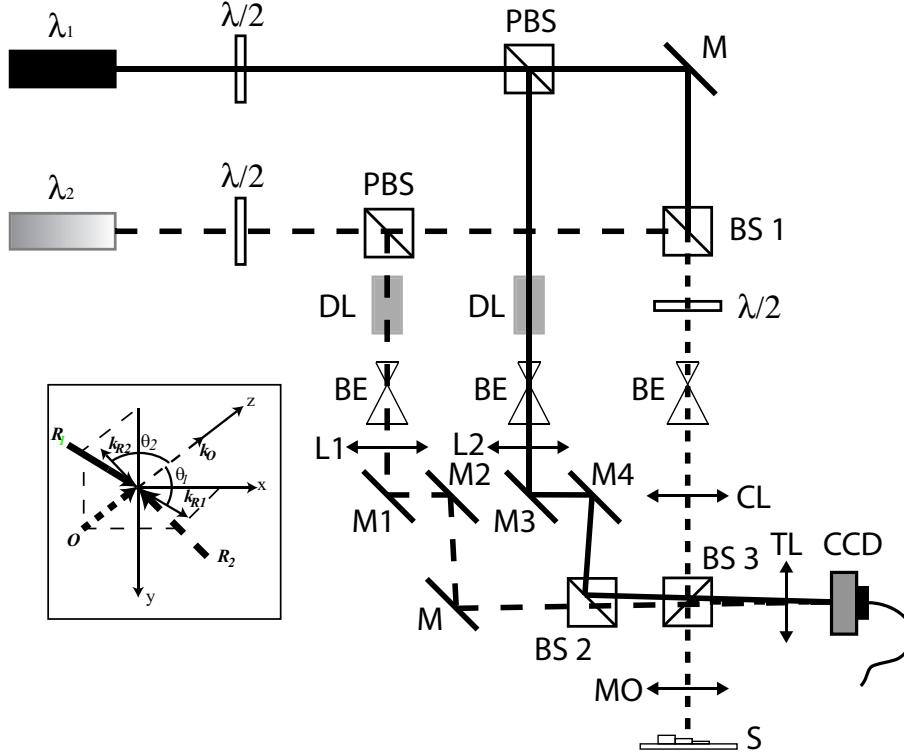


Figure 1. Two-wavelengths DHM setup. $\lambda/2$: half-waveplate, M: mirrors, PBS: polarizing beamsplitter, BS: non-polarizing beamsplitter, DL: delay line, BE: beam-expander, L: lens, CL: condenser lens, MO: x3 achromatic microscope objective, 0.1 NA, S: specimen, TL: tube lens; Inset: 3D distribution of the incident waves propagation directions upon the CCD plane, k_{R1} and k_{R2} are the propagation direction vector of the reference waves R_1 for wavelength λ_1 and R_2 for λ_2 .

The principle of this setup is to separate both laser beams, of different wavelengths, in different reference arms, while aligning and combining them in an achromatic object arm. Both collinear reflected object wavefronts are collected by the MO (infinity-corrected), and the object images are formed by the tube lens (focal 150mm) about 50mm behind the CCD plane. A low magnification x3 MO, with a NA of 0.1, is used in the present case to achieve large field-of-view (FOV), $1\text{x}1\text{mm}^2$ with $512\text{x}512$ pixels, and a depth-of-field (DOF) of more than $50\mu\text{m}$. Of course it is important that the DOF exceeds the beat-wavelength phase measurement range, but there is no theoretical limitation regarding the use of higher magnification. The CCD camera is a standard 8 bits black and white CCD camera with $6.45\mu\text{m}$ pixel size. Each reference arm comprise a delay line (DL), which can be adjusted to match the optical path length of its respective object counterpart, in order to obtain an interference on the CCD for both wavelengths. By tilting the pair of mirrors M1 and M2 for the first wavelength reference beam, respectively M3 and M4 for the second one, each k-vector incident upon the CCD camera can be finely tuned. In other words, it is possible to set up each wavelength interferograms fringes both in spatial frequency and orientation.

The ideal configuration for dual-wavelength DHM is depicted in the inset of Fig. 1, with orthogonal spatial frequencies for each wavelength interferogram. This arrangement ensures an optimum repartition of the interference terms in the hologram Fourier domain, and it minimizes overlaps between the spatially-multiplexed terms. An example of dual-wavelength hologram and its Fourier spectrum are represented in Fig. 2, with the real and virtual images components for each wavelength interferogram and the orthogonal fringes regimes.

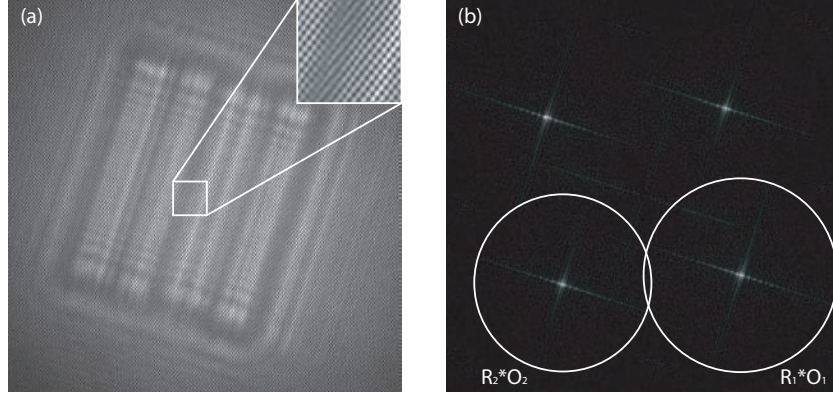


Figure 2. (a) Two-wavelengths spatially-multiplexed hologram with the inset representing a zoom on the central fringes, where the orthogonal spatial frequencies can be seen; (b) Fourier-spectrum of (a) (the zero order is filtered), where the virtual images for each wavelength can be separately spatial-filtered (red = 760nm, green = 680nm)

As illustrated in Fig. 2, the orthogonal repartition of the spatial frequencies enables to filter (select) separately the interference term of each wavelength in the Fourier spectrum of the hologram. In other words, the real image components $R_i O_i^*$, or the virtual image components $R_i^* O_i$, or any other set of interference terms, can be selected independently as depicted in Fig. 2(b). This experimental configuration for recording holograms is very similar to the one in Ref. [19, 20] and permits to encode multiple wavefronts with only a single acquisition thanks to different carrier frequencies. A transverse resolution of $4.4\mu\text{m}$ has been measured with a USAF 1950 resolution test target and the system is diffraction-limited according to the NA of the MO.

Having selected each wavelength interference term, here the two virtual images components, one can use Eq. 2 to reconstruct and propagate each wavefront in the convolution formalism. By correcting for aberrations in the hologram plane before the propagation, especially the tilt, the reconstructed images are naturally centered [9]. This perfect superposition and the achromatic design of the object arm of the setup, allow for an accurate subtraction of the wavefronts in the image plane. The reconstruction distances in the experimental configuration of Fig. 1 are $d_1 = 50\text{mm}$ for $\lambda_1 = 680\text{nm}$ and $d_2 = 50.5\text{mm}$ for $\lambda_2 = 760\text{nm}$ and they correspond to the distances between the image planes and the CCD camera plane. As the reconstruction distances difference is very small due to the achromatic conditions, the magnification difference can be considered negligible and the images superposition is excellent.

For this setup, a high quality mirror has permitted to evaluate an experimental noise of about 2 degrees of phase spatial standard deviation over the whole field-of-view in phase for each wavefront. Interestingly, this spatial standard deviation value is the same as for single-wavelength DHM. When considering the synthetic beat phase Φ , the spatial standard deviation raises to about 3 degrees, which corresponds to a $\sqrt{2}$ amplification typical for the sum of two Gaussian-noise distributions. In terms of axial topographic resolution, this corresponds to about 2nm precision for monochromatic phases, and 27nm for the beat-wavelength phase precision, which is a consequence of the noise amplification phenomena.

4. RESULTS

To assess the technique, a purely-reflective object with abrupt steps of more than half a visible-range wavelength in height will be investigated. Such a specimen usually cannot be measured with monochromatic DHM because the phase ambiguity is nearly impossible to solve with the help of unwrapping algorithms, due to the steep transitions compared to the lateral resolution. This sample is a micro-structured SiO₂ staircase on a Si wafer with a gold coating to ensure a perfect reflectivity. It consists in five steps with the following height values: 375, 525, 975, 1200, 1275nm inducing up to 2.5 μ m in term of OPL, which represents about four times a typical red-range wavelength and out of range of classical single-wavelength DHM. A schematic of this test-object and experimental reconstruction images, in amplitude and phase, of this sample from the hologram of Fig. 2 with the setup of Fig. 1 are presented in Fig. 3

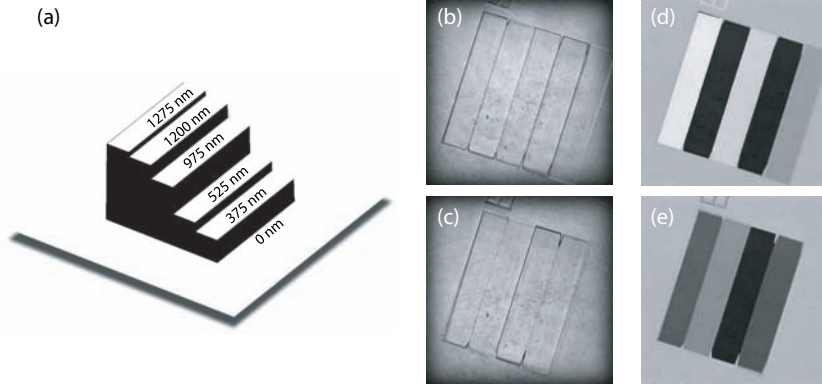


Figure 3. (a) Schematic of the staircase test-sample; (b,c) amplitude and (d,e) phase of respectively the reconstructed wavefront O_1 ($\lambda_1 = 680\text{nm}$, $d_1 = 5\text{cm}$) and O_2 ($\lambda_2 = 760\text{nm}$, $d_2 = 5.05\text{cm}$) obtained from the hologram of Fig. 2 (grayscale: black = -180, white = +180 for the phase; field-of-view: $1\times 1\text{mm}^2$)

The two phase-contrast images of the staircase object in Fig. 3(d,e) obtained from the recorded hologram (Fig. 2) illustrate well the phase ambiguity for single-wavelength imaging: the smallest step of 375nm disappears in Fig. 3(e) because it corresponds to an OPL of 750nm, which is nearly the value of $\lambda_2 = 760\text{nm}$. This is a typical case where unwrapping algorithms are helpless. But now as we have recorded both wavelengths wavefronts with the same hologram acquisition, one can compute the phase difference between Figs. 3(d) and 3(e) according to Eq. 3. After inverting the sign of the phase to obtain a topographic map, corresponding to a conjugated phase map), and as will be done for all synthetic phase-maps further on, we have the $\Lambda = 6.428\mu\text{m}$ synthetic wavelength topographic map of Fig. 4.

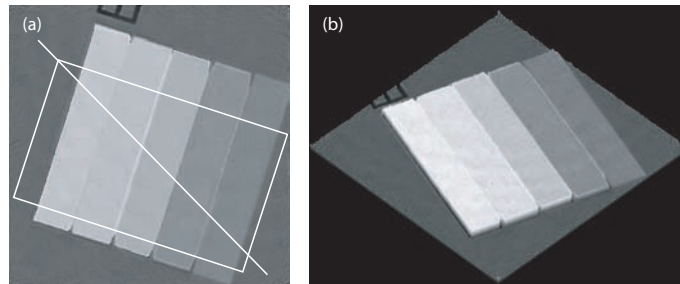


Figure 4. Single-hologram beat-wavelength conjugated phase map of the sample of Fig. 3 at $\Lambda = 6.428\mu\text{m}$ (grayscale: black = -180, white = +180). (a) Synthetic phase-contrast image of the Si staircase sample at $\Lambda = 6.428\mu\text{m}$; (b) 3D perspective of (a).

The measurement of this sample with a synthetic wavelength of $\Lambda = 6.428\mu\text{m}$ provides a phase jumps-free result and a real 3D topographic map of this up to 1.275 μm high specimen as can be seen in Fig. 4(b). In order

to validate the method, profiles measurements are extracted on the synthetic map of Fig. 4 and the results are presented in Fig. 5 with a comparison with white light interferometer data on the same object.

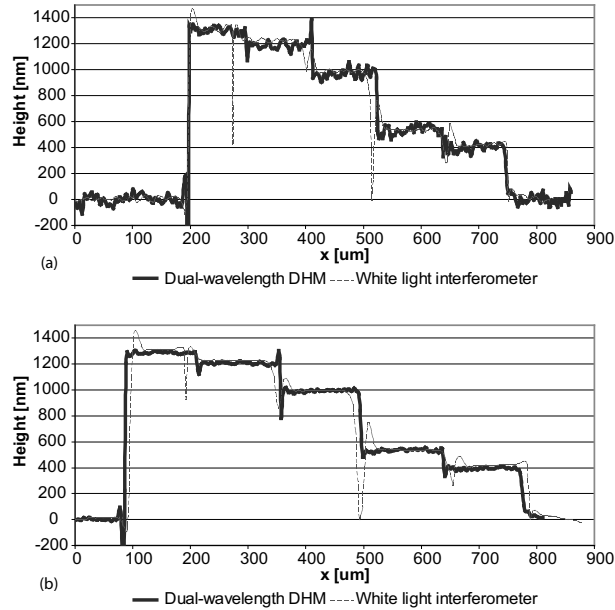


Figure 5. (a) 1-D profiles taken along the white line in Fig. 4(a) superposed with a profile obtained with a commercial white light interferometer; (b) spatial average of about 100 profiles taken perpendicular to the small edge of the white rectangle in Fig. 4(a) compared with a similar spatial average profile with the white light interferometer measurements.

Fig. 5 results indicates that the quantitative experimental measurements with two-wavelengths DHM are in agreement with the white-light interferometry comparative measurements, plus they are within the manufacturing error of 2% of the theoretical topographic values. Moreover, as illustrated in Fig. 5(b), the precision can be enhanced by spatially averaging profiles, and in this case the measure seems even more accurate than with the white light interferometer.

The real-time capability is however the main added-value of the method, and is especially useful for moving samples measurements like e.g. moving MEMS/MOEMS parts monitoring either in real-time or in stroboscopic mode [26]. To illustrate this advantage of the technique, we have chosen to characterize a $4 \times 4 \text{mm}^2$ oscillating micro-mirror at a frequency of 1Hz. Fig. 6 presents phase reconstruction results for a single wavelength [Fig. 6(a)] and for the $\Lambda = 6.428 \mu\text{m}$ synthetic wavelength [Fig. 6(b)] when the micro-mirror is at the maximum deflection ($t=0.5\text{s}$).

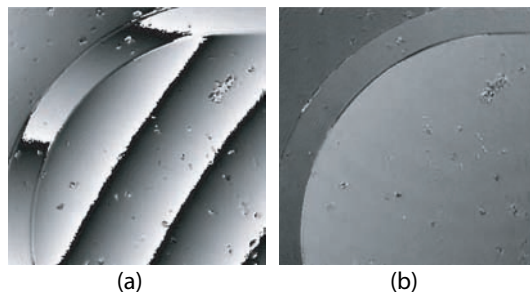


Figure 6. Dual-wavelength phase measurements on a moving micro-mirror oscillating at 1Hz during 6s (at 25 frames/s). (grayscale: black = -180, white = +180; field-of-view: $1 \times 1 \text{mm}^2$) (a) Phase-contrast image at $t=0.5\text{s}$ for the wavelength $\lambda_1 = 680\text{nm}$; (b) Phase-contrast image at $t=0.5\text{s}$ for the beat wavelength $\Lambda = 6.428 \mu\text{m}$.

Figure 6(b) shows clearly the advantages of synthetic wavelength imaging for such moving micro-parts investigation, with results free of phase jumps. To quantitatively monitor the moving part during the whole sequence, Figure 7 provides topographic profile lines taken through one of the corner of the moving mirror. The field-of-view (FOV) of $1 \times 1 \text{mm}^2$ is about a quarter of the complete mirror and the measurements, obtained at video-frequency (25 frames/s) are presented for half-a-period of oscillation (0.5s).

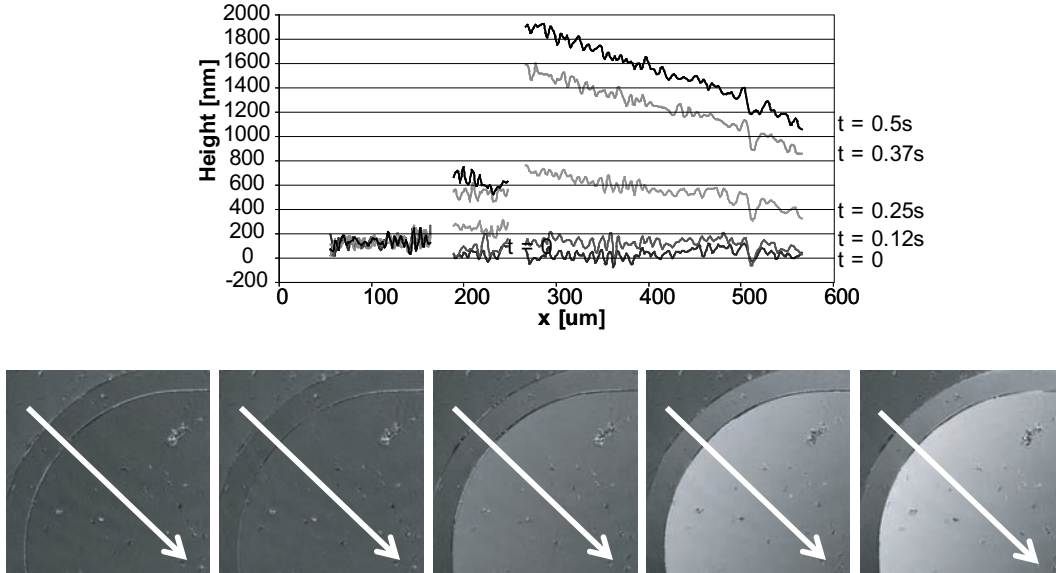


Figure 7. Half-a-period monitoring of micro-mirror movements at the wavelength $\Lambda = 6.428 \mu\text{m}$ synthetic wavelength

5. CONCLUSION

We proposed a technique to achieve real-time dual-wavelength digital holographic microscopy with a single hologram acquisition. The principle of the method is based on the use of multiple reference waves with a spatial multiplexing of the hologram by incoherent addition of single-wavelength interferograms. The two different wavelength laser beams are mixed in the object arm while each reference waves are kept separated and have different incident angles for the hologram recording. The properties of off-axis digital holography permit to separately extract the spatial frequencies associated to each wavefront in the Fourier domain, and then to propagate the corresponding wavefronts in parallel. At this point the phase difference can be computed and thus the reconstruction of the synthetic wavelength phase distribution of a reflective object is achieved with a single acquisition. This enables to increase dramatically the dynamic range of phase measurements and to remove the phase ambiguity of single-wavelength digital holography. Results to assess the method on a $1.2 \mu\text{m}$ high test-target with a $6.4 \mu\text{m}$ synthetic wavelength are in good agreement with white light interferometer measurements. Furthermore, to illustrate the real-time capability advantage of our technique, quantitative measurements on a 1Hz oscillating micro-mirror at video frequency acquisition have been presented.

The development of the technology has been supported by Swiss government through CTI grants TopNano 21 #6101.3 and NanoMicro #6606.2 and #7152.1. The author would like to thank the staff of Lyncee Tec SA (www.lynceetec.com) for their collaboration and the fruitful contributions.

REFERENCES

1. J. W. Goodman and R. W. Lawrence, "Digital image formation from electronically detected holograms," *Appl. Phys. Lett.* **11**(3), pp. 77–79, 1967.
2. U. Schnars and W. Jüptner, "Direct recording of holograms by a ccd target and numerical reconstruction," *Appl. Opt.* **33**(2), pp. 179–181, 1994.

3. E. CuChe, F. Bevilacqua, and C. Depeursinge, "Digital holography for quantitative phase-contrast imaging," *Opt. Lett.* **24**(5), pp. 291–293, 1999.
4. D. Gabor, "A new microscopic principle," *Nature* **161**(4098), pp. 777–778, 1948.
5. E. CuChe, P. Marquet, and C. Depeursinge, "Simultaneous amplitude-contrast and quantitative phase-contrast microscopy by numerical reconstruction of fresnel off-axis holograms," *Appl. Opt.* **38**(34), pp. 6994–7001, 1999.
6. C. Wagner, W. Osten, and S. Seebacher, "Direct shape measurement by digital wavefront reconstruction and multiwavelength contouring," *Optical Engineering* **39**(1), pp. 79–85, 2000.
7. J. Gass, A. Dakoff, and M. K. Kim, "Phase imaging without 2 pi ambiguity by multiwavelength digital holography," *Opt. Lett.* **28**(13), pp. 1141–1143, 2003.
8. D. Parshall and M. Kim, "Digital holographic microscopy with dual wavelength phase unwrapping," *Appl. Opt.* **45**(3), pp. 451–459, 2006.
9. T. Colomb, F. Montfort, J. Kühn, N. Aspert, E. CuChe, A. Marian, F. Charrière, S. Bourquin, P. Marquet, and C. Depeursinge, "Numerical parametric lens for shifting, magnification and complete aberration compensation in digital holographic microscopy," *J. Opt. Soc. Am. A* **23**(12), pp. 3177–3190, 2006.
10. S. de Nicola, A. Finizio, G. Pierattini, D. Alfieri, S. Grilli, L. Sansone, and P. Ferraro, "Recovering correct phase information in multiwavelength digital holographic microscopy by compensation for chromatic aberrations," *Opt. Lett.* **30**(20), pp. 2706–2708, 2005.
11. I. Yamaguchi, K. Yamamoto, G. A. Mills, and M. Yokota, "Image reconstruction only by phase data in phase-shifting digital holography," *Appl. Opt.* **45**(5), pp. 975–983, 2006.
12. R. J. Mahon, J. A. Murphy, and W. Lanigan, "Digital holography at millimetre wavelengths," *Opt. Commun.* **260**(2), pp. 469–473, 2006.
13. F. Zhang, G. Pedrini, and W. Osten, "Reconstruction algorithm for high-numerical-aperture holograms with diffraction-limited resolution," *Opt. Lett.* **31**(11), pp. 1633–1635, 2006.
14. A. W. Lohmann, "Reconstruction of vectorial wavefronts," *Appl. Opt.* **4**(12), pp. 1667–1668, 1965.
15. E. N. Leith and J. Upatnieks, "Wavefront reconstruction with diffused illumination and three-dimensional objects," *J. Opt. Soc. Am.* **54**(11), pp. 1295–1301, 1964.
16. E. N. Leith and J. Upatnieks, "Wavefront reconstruction with continuous-tone objects," *J. Opt. Soc. Am.* **53**(12), pp. 1377–1381, 1963.
17. J. D. Armitage and A. W. Lohmann, "Theta modulation in optics," *Appl. Opt.* **4**(4), pp. 400–403, 1965.
18. D. Beghuin, E. CuChe, P. Dahlgren, C. Depeursinge, G. Delacretaz, and R. P. Salathe, "Single acquisition polarisation imaging with digital holography," *Electron. Lett.* **35**(23), pp. 2053–2055, 1999.
19. T. Colomb, P. Dahlgren, D. Beghuin, E. CuChe, P. Marquet, and C. Depeursinge, "Polarization imaging by use of digital holography," *Appl. Opt.* **41**(1), pp. 27–37, 2002.
20. T. Colomb, E. CuChe, F. Montfort, P. Marquet, and C. Depeursinge, "Jones vector imaging by use of digital holography: simulation and experimentation," *Opt. Commun.* **231**(1-6), pp. 137–147, 2004.
21. A. T. Saucedo, F. M. Santoyo, M. D. I. Torre-Ibarra, G. Pedrini, and W. Osten, "Endoscopic pulsed digital holography for 3d measurements", *Opt. Lett.* **14**, 1468–1475 (2006).
22. T. Saucedo A., F. M. Santoyo, M. D. I. T. Ibarra, G. Pedrini, and W. Osten, "Simultaneous two-dimensional endoscopic pulsed digital holography for evaluation of dynamic displacements", *Appl. Opt.* **45**, 4534–4539
23. E. CuChe, P. Marquet, and C. Depeursinge, "Spatial filtering for zero-order and twin-image elimination in digital off-axis holography," *Appl. Opt.* **39**(23), pp. 4070–4075, 2000.
24. T. Colomb, E. CuChe, F. Charrière, J. Kühn, N. Aspert, F. Montfort, P. Marquet, and C. Depeursinge, "Automatic procedure for aberration compensation in digital holographic microscopy and applications to specimen shape compensation," *Appl. Opt.* **45**(5), pp. 851–863, 2006.
25. P. de Groot and S. Kishner, "Synthetic wavelength stabilization for two-color laser-diode interferometry," *Appl. Opt.* **30**(28), pp. 4026–4033, 1991.
26. Y. Emery, E. CuChe, F. Marquet, N. Aspert, P. Marquet, J. Kühn, M. Botkine, T. Colomb, F. Montfort, F. Charrière, C. Depeursinge, P. Debergh, and R. Conde, "Digital holographic microscopy (DHM) for metrology and dynamic characterization of MEMS and MOEMS", *Proc. SPIE* **6186**, N1860–N1860 (2006).